pagepress

Journal of Limnology

Journal of Limnology 2026; 85(s1):2281
doi:10.4081/jlimnol.2026.2281

©Copyright: the Author(s), 2026
Licensee PAGEPress, Italy

Enhancing shallow water habitat mapping with high-resolution pansharpened PRISMA imagery data

Lodovica Panizza,[1]* Mariano Bresciani,[1] Alessia Tricomi,[2] Federica Braga,[3] Andrea Pellegrino,[1,4] Alice Fabbretto,[1] Riccardo Musto,[5] Cecilia Sciarretta,[6] Claudia Giardino[1]

[1]National Research Council-Institute for Electromagnetic Sensing of the Environment (CNR-IREA), Milan; [2]e-GEOS S.p.A., Rome; [3]National Research Council-Institute of Marine Sciences (CNR-ISMAR), Venice; [4]Department of Engineering, Sapienza University of Rome; [5]Leonardo Labs (Leonardo S.p.A.), Rome; [6]Telespazio/e-GEOS S.p.A., Rome, Italy

Abstract

Macrophytes are crucial elements in freshwater ecosystems and ecological processes, by supporting biodiversity, stabilizing sediments, and improving water quality. Nowadays, these ecosystems are threatened by environmental changes and the increase in anthropic pressures; moreover, their spatial distribution is often highly fragmented. Considering their importance, monitoring macrophytes' spatio-temporal variability with non-invasive observations is fundamental. Hyperspectral remote sensing offers a valuable tool for mapping aquatic vegetation and benthic substrates accurately, although its application is often limited by spatial resolution, especially in environments characterized by patch distribution and mixed pixels. To address these limits, this study exploits the PRISMA panchromatic band for a PRISMA image acquired on 09/07/2024 on Lake Garda (Italy), combining high spectral resolution (66 band in the visible-near-infrared range) with enhanced spatial resolution (5 m). The pansharpening procedure is applied to PRISMA Level 2D images using a deep learning model trained through both supervised and unsupervised learning techniques. This study focuses on the optically shallow waters of the Sirmione Peninsula (southern portion of Lake Garda), characterized by the presence of macrophytes coverage, with the goal of classifying the benthic substrate into seven classes, and retrieving bottom depth. In addition to the panchromatic product with a spatial resolution of 5 m, aggregated products with resolutions of 10 m and 30 m were also generated. The results showed overall accuracies of 80%, 68%, and 48% for resolutions ranging from 5 m to 30 m in the classification of the benthic substrate. Similar results were obtained in the validation of bottom depths when compared to data collected by the Institute of the Italian Navy (IIM) and *in situ* measurements acquired during the field campaign (r=0.82 for 5 m data, r=0.78 for 10 m data, r=0.75 for 30 m data). The outcomes enable more accurate monitoring of spatial-temporal dynamics in freshwater ecosystems and highlight the potential of pansharpened hyperspectral products to enhance the mapping and classification of benthic substrates, with higher accuracy in detecting small patches.

Key words: Inland water; imaging spectroscopy; high-resolution; bio-optical model; pansharpening; macrophytes.

**Correspondence to: panizza.l@irea.cnr.it*

INTRODUCTION

Aquatic macrophytes are key components of freshwater ecosystems, contributing to both structure and function (Thomaz *et al*., 2025). They include various plant forms (submerged, floating, and emergent) and play a central role in shaping ecological processes, from habitat formation to biogeochemical cycling. By increasing habitat complexity in the littoral zone (Meerhoff and de los Ángeles González-Sagrario, 2021), they support biodiversity by providing refuge, nursery areas, and feeding grounds for invertebrates, fish, and microbial communities, while also stabilizing sediments and improving water clarity (Lesiv *et al*., 2020).

They are also crucial for nutrient cycling, acting as sinks for nitrogen and phosphorus, enhancing oxygenation, and limiting phytoplankton growth, thereby helping maintain clear-water conditions. Additionally, they contribute to carbon sequestration and overall ecosystem metabolism (Thomaz, 2023). However, macrophyte communities are highly vulnerable to environmental pressures such as eutrophication, hydrological changes, and climate change (Bertrin *et al*., 2018; Park *et al*., 2024). A major and growing threat is the spread of invasive benthic species, which can outcompete native macrophytes, alter habitat structure, and disrupt trophic interactions. These invasions may lead to reduced biodiversity, modified nutrient dynamics, and shifts in ecosystem stability, sometimes reinforcing further invasions or degradation (Villamagna and Murphy, 2010). Macrophyte distribution is also influenced by anthropogenic and environmental factors. In particular, boats and recreational vessels can strongly influence the patch distribution of macrophytes in lakes and coastal areas by introducing both physical disturbance and hydrodynamic changes, which alter how vegetation is spatially organized (Asplund and Cook, 1997; Sagerman *et al*., 2020).

Considering that macrophytes are important biological indicators of water and sediment quality, monitoring their distribution is

OPEN ACCESS

crucial as they reflect environmental conditions. Standard traditional approaches typically show some limits in scale, frequency, and costs. Remote sensing has become a key tool for conservation, management, and research of critical benthic ecosystems (Bell *et al*., 2023; Schütt *et al*., 2025), enabling large-scale, repeatable, and non-invasive observations. In particular, the use of multispectral and hyperspectral sensors allows the mapping of aquatic vegetation and benthic substrates, as well as the estimation of key properties such as biomass, cover, structural complexity and species composition on the basis of their spectral signatures (Ghirardi *et al*., 2019). Despite its advantages, remote sensing faces technical challenges, particularly in the analysis of submerged or flooded vegetation, where water column effects can distort spectral signals. Spatial resolution is one of the primary limiting factors for remote sensing applications in freshwater ecosystems, as coarse-resolution data may result in mixed pixels that combine different environmental features, thereby reducing the ability to characterize their spatial distribution and regression or expansion over time (Gasith and Hoyer, 1998; Olmanson *et al*., 2015). This limitation is particularly relevant for macrophyte mapping, as vegetation are often spatially heterogeneous and may include multiple species with gradual boundaries, or more species present in a small area. This heterogeneity can result in vegetation patches surrounded by bare areas, transitions between fine and coarse sediments, and gradients between nutrient-rich and nutrient-poor zones (Schoelynck *et al*., 2018). Higher spatial and spectral resolution can therefore improve the discrimination of vegetation patches and other aquatic features. However, even at high spatial and spectral resolution, additional issues such as turbidity and signal attenuation may further complicate data interpretation. These challenges highlight the importance of combining ongoing remote sensing technological advancements with *in situ* measurements to improve the accuracy and reliability of aquatic ecosystems monitoring (Ghirardi *et al*., 2022).

In the last few years, hyperspectral spaceborne and airborne images have been providing significant advances in algorithm development and innovative mapping tools (Belluco *et al*., 2006; Hestir *et al*., 2008; O'Shea *et al*., 2021; Begliomini *et al*., 2023; Giardino *et al*., 2025). To overcome the limit induced by the low spatial resolution, an approach can be the fusion of hyperspectral images with high-resolution panchromatic imagery. In this regard, the PRecursore IperSpettrale della Missione Applicativa (PRISMA) mission is equipped with two sensors: a hyperspectral camera with 30 m spatial resolution and a panchromatic camera with 5 m spatial resolution. Combining data derived from the two cameras through the procedure of pansharpening, a single product characterized by high spatial and spectral resolution can be obtained to support a variety of applications, including floating matter detection (Taggio *et al*., 2022; Corbari *et al*., 2023).

The main challenge is to design a fusion model capable of generating high quality results while enhancing spatial resolution and preserving spectral accuracy. A wide range of methods have been proposed for pansharpening, with many approaches adapting techniques originally developed for the multispectral domain. Classical pansharpening algorithms can be divided into four categories: component substitution (CS), multiresolution analysis (MRA), hybrid, and Bayesian (Alparone, 2015; Loncan *et al*., 2015; Vivone *et al*., 2015).

Over the past decade, deep learning has gained significant traction across various research domains, including remote sensing, largely due to its capacity to model complex nonlinear relationships. An approach based on Convolutional Neural Network (CNN) was introduced in Masi *et al*. (2016), which represents the foundation for subsequent techniques developed in the following years (Yang *et al*., 2017; He *et al*., 2019, 2020; Zheng *et al*., 2020; Bandara *et al*., 2021).

The study area of this work is the Sirmione Peninsula, located in the southern portion of Lake Garda (northern Italy). This area features numerous unique habitats, such as common reed beds and extensive submerged macrophyte meadows, in addition to the most diverse population of overwintering waterbirds in Italy (Bresciani *et al*., 2011; Villa *et al*., 2013). The lake is an example of a multifunctional territorial system in which ecology and economy are deeply interconnected. It plays a critical role in regional climate buffering, mitigating extreme temperatures (Salmaso *et al*., 2018), biodiversity conservation (Bolpagni *et al*., 2013), water resources management (Hinegk *et al*., 2023), tourism, agriculture (Badiani *et al*., 2017), and energy production. Several analyses have been carried out on the macrophytes expansion in this lake; Ghirardi *et al*. (2022) for example, evaluated the macrophyte community dynamics in terms of spatial extent and density in the southern portion of Lake Garda using Sentinel-2, for the period 2015-2020. The possible effect of the COVID-19 was also analyzed, particularly in the areas associated with boat transit where a recovery in macrophyte coverage was registered.

The aim of this study is to evaluate the benefits of characterizing Lake Garda shallow water areas using an improved spatial resolution of 5 m, obtained by fusing the visible-near-infrared (VNIR) hyperspectral data cube provided by PRISMA (spatial resolution of 30 m) with the corresponding 5 m panchromatic image. This work addresses the well-known mismatch between the spatial scale of satellite hyperspectral observations and the fine-scale heterogeneity of macrophyte-dominated environments; the ideal spatial resolution for mapping and monitoring aquatic vegetation is identified in fact as less than or equal to 5 m (Roelfsema *et al*., 2014; Dierssen *et al*., 2023). In this context, we investigated the impact of spatial resolution on both benthic substrate classification and bathymetric retrieval, providing a multi-scale assessment of product performance through validation with *in situ* measurements. In addition, shallow water products were aggregated to 10 m and 30 m spatial resolution, to be consistent with freely available optical satellite sensors commonly used for shallow water applications at different spatial scales.

METHODS

Study area

Lake Garda, the largest lake in Italy, represents a system of outstanding environmental and economic significance within the Southern Alpine region. Situated between the regions of Lombardy, Veneto, and Trentino-Alto Adige, with an area of 370 km^2, a water volume of 50 km^3 and a maximum depth of 346 m, the lake constitutes a complex socio-ecological system in which natural processes and human activities are closely intertwined (Giardino *et al*., 2007b; Salmaso and Padisák, 2007). Lake Garda can be classified as oligo-mesotrophic; in the epilimnion, phosphorus levels remain at or below 10 µg/L, Chlorophyll-a (Chl-a) averages around 3 mg/m^3, and water transparency varies markedly through the year, with Secchi depths of 4–5 m in summer and 15–17 m in late winter (Giardino *et al*., 2014).

From a morphological perspective, the basin is composed of two distinct sectors: a broad northern–southwestern sub-basin with the deepest areas, and a shallower sub-basin located to the southeast.

OPEN ACCESS

The northern shores are bordered by steep mountain slopes dominated by forested or rural landscapes, whereas the southern sector transitions into morainic and alluvial plains, low hills, and a mosaic of urban and rural land use (Salmaso and Mosello, 2010).

From an environmental perspective, Lake Garda is characterized by high ecological diversity, resulting from its geographic position at the interface between the Alpine and Mediterranean biogeographical zones (Salmaso *et al*., 2018). This transitional location creates a unique microclimate, moderated by the large water mass, which supports a wide range of plant and animal species. The surrounding habitats include subalpine forests, Mediterranean scrublands, wetlands, and agricultural landscapes, forming a mosaic that enhances ecological connectivity and resilience. The lake itself hosts diverse aquatic communities, including endemic and economically important fish species (Ciutti *et al*., 2011).

Lake Garda is the second most visited Italian destination; the tourism activity sustains local employment and stimulates related sectors, including transportation, retail, and services. In addition to tourism, the lake basin supports high value agricultural production, particularly viticulture and olive cultivation (Goffi *et al*., 2021). Overall, the lake represents a strategic freshwater reservoir, used for drinking supply, irrigation, and industrial purposes, supporting both urban centers and rural areas, although the increasing anthropogenic pressures pose significant challenges to water quality and ecosystem integrity (Hinegk *et al*., 2022). Additionally, the lake's outflow system is integrated into hydroelectric infrastructure, contributing to renewable energy generation.

PRISMA data

The PRISMA mission, operated by the Italian Space Agency, is a hyperspectral satellite mission that combines a hyperspectral (HYC) camera acquiring 239 contiguous spectral bands ranging from 400 to 2500 nm with a 30 m Ground Sampling Distance (GSD), and a medium-resolution panchromatic (PAN) camera with 5 m GSD, using pushbroom scanning technique (Loizzo *et al*., 2018; Cogliati *et al*., 2021). The PRISMA products include Level 1 (L1), and Level 2 (L2), which differ by processing levels, ranging from Top-of-Atmosphere (TOA) radiance obtained through radiometric calibration and corrections such as cloud and sunglint masking (L1), to Bottom-of-Atmosphere (BOA) reflectance derived from TOA spectral measurements after atmospheric correction (L2) (Pellegrino *et al*., 2023). Since the PAN camera is co-registered with HYC data, it enables the evaluation and application of image fusion techniques (Aiazzi *et al*., 2013; Vivone *et al*., 2023; Musto *et al*., 2024; Ziaja *et al*., 2025) as well as finer scale mapping (Kapakasa *et al*., 2024). For the purposes of this study, the HYC and PAN PRISMA products acquired over the Sirmione Peninsula on 9th July 2024 were used.

Pansharpening processing

The pansharpening procedure is applied to PRISMA Level 2D image using a deep learning model trained through both supervised and unsupervised learning strategies. The training steps follow a slightly modified version of the approach reported in Musto *et al*. (2023).

Typically, deep learning approaches are based on Wald's protocol (Wald *et al*., 1997). This protocol is widely adopted because *in situ* data at full resolution are generally unavailable, making supervised training and quantitative evaluation of fused images difficult. It involves downsampling both hyperspectral data and the panchromatic image before using them as input for training the model, with the original hyperspectral data serving as a reference. The key assumption is scale invariance that does not consistently hold in practice, leading to potentially low performance when applying the trained models to full resolution data. To address this limitation, Musto *et al*. (2023) introduced a synthetic dataset generated from Airborne Visible-Infrared Imaging Spectrometer - Next Generation (AVIRIS-NG) data, enabling fully supervised training. AVIRIS-NG is an imaging spectrometer that acquires spectral information across a wide wavelength range, from 380 nm to 2510 nm, with a spectral resolution of 5 nm over 425 channels. Consequently, AVIRIS-NG flights with a spatial resolution in the range [0, 6] m have been used to generate the synthetic dataset. The flights have been selected from various locations across Europe, such as Italy, Germany and Switzerland, ensuring a wide variety of both spectral and spatial detail. Due to its high spatial and spectral resolution, AVIRIS-NG data can be resampled to simulate PRISMA-like observations, generating a high-resolution hyperspectral dataset (5 m), a synthetic panchromatic image (5 m), and a low-resolution hyperspectral dataset (30 m). These data provide a high-resolution hyperspectral reference for fully supervised training, avoiding the scale-invariance assumption of the Wald protocol.

Two distinct modules were implemented, and both employ a lightweight Convolutional Neural Network (CNN). Initially, the model is trained in a supervised mode using AVIRIS-NG data. Subsequently, the model undergoes unsupervised training directly on PRISMA data, which refines the spectral reconstruction and minimizes distortions as in Ciotola *et al*. (2022). This dual-step approach leverages the strength of both sensor types, offering a solution to improve the spatial resolution of hyperspectral imaging, preserving the spectral quality. The CNN architecture is composed of three branches, each devoted to a specific function. The upper branch focuses on preserving spectral information of the hyperspectral cube, while the lower branch is dedicated to the extraction of spatial details from the panchromatic image, and the central branch is designed for upscaling the hyperspectral cube. The quality of the pansharpening process was assessed using the Hybrid Quality (HQNR) protocol (Vivone *et al*., 2021; Arienzo *et al*., 2022), that resulted with a HQNR score of 0.87, hence close to its maximum value of 1. The quality controlled pansharpened PRISMA product with a 5 m pixel size, was then reduced to a data cube that consists of 66 bands in the VNIR range, as only a subset of the available spectral information was required for the subsequent analysis. The selected bands covered the wavelength range from 406 to 1010 nm. The BOA reflectance was divided by π to obtain remote sensing reflectance values (Rrs, in sr^{-1} units) independent of the specific geometry of the Sun and sensor, as well as atmospheric conditions (Giardino *et al*., 2007a). Rrs data were then used as input to the algorithms for shallow water property retrieval.

In situ data

To assess the quality of the PRISMA Rrs pansharpened product (PRISMA pansh) and related shallow water products, a field campaign in coincidence with PRISMA overpass was performed (Ruddick *et al*., 2024a; 2024b; Rubio *et al*., 2025).

The measurements conducted during the field campaign included the collection of Rrs acquired with different hand-held spectroradiometers: WISP-3 and WISP-Orca (Water Insight, Wageningen, The Netherlands) (Hommersom *et al*., 2012), and Spectral Evolution (SR-3500) (Vabson *et al*., 2019). WISP-3 and WISP-Orca perform automatically measurements with three radiometers that simultaneously measure water and sky radiances at 40° at Nadir, and total irra-

diance (Braga *et al*., 2013; Giardino *et al*., 2014). The spectroradiometers operate in the spectral range of 380–800 nm with a bandwidth of 4.9 nm. Each acquisition consists of five measurements per radiometer and typically takes between 30 and 90 sec, depending on illumination conditions. On the other hand, the SR-3500 uses a single spectrometer equipped with interchangeable entrance optics for irradiance and radiance and can be used subsequently to measure both upwelling and downwelling radiance. Its spectral range is 350-2500 nm, with different spectral resolutions depending on the spectral region (3 nm in the range 350-1000 nm). Measurements were sequentially acquired by mounting a remote cosine receptor and a 5° lens and keeping the angles consistent to the SeaWiFS protocol (Mueller *et al*., 2000).

Fig. 1 provides the map of the stations collected during the field campaign on 9th July 2024. At nine stations (blue diamonds), spectral measurements (SM) were collected using WISP-3, WISP-Orca, and the SR-3500, with multiple acquisitions performed at each station and subsequently averaged to reduce noise. At 32 stations (orange circles) along the Sirmione Peninsula, bottom classification (BC), water depth, and GPS positions were recorded. At nine of these 32 stations, bottom sediment and vegetation samples were collected for ex-situ radiometric measurements of recency. Vegetation was sampled using a 0.25 m^2 hoop positioned above the macrophyte meadow (Bresciani *et al*., 2012), with three replicates at each station to characterize the predominant bottom types rather than to provide a quantitative estimate of macrophyte cover within the entire PRISMA pixel. For the ex-situ radiometric measurements, a contact probe was attached to the SR-3500 for the characterization of bottom reflectance of the predominant vegetated bottom type classes (Fig. 2). Furthermore, bathymetric data gathered from a high-resolution survey from the Hydrographic Institute of the Italian Navy (IIM) was available for validating PRISMA-derived bottom depths.

Bio-optical modelling

The PRISMA pansh image storing the Rrs data was directly used as input of a non-linear optimization algorithm, for simultaneously assessing the fractional cover (fc) of substrate types and depths. The algorithm builds on Lee *et al*. (1999) and it is implemented as an ENVI add-on tool: Bio-Optical Model-Based tool for Estimating water quality and bottom properties from Remote sensing images (BOMBER) (Giardino *et al*., 2012). Through a spectral reflectance inversion, it enables the retrieval of bottom depth and the coverage distribution of up to three types of substrates. The BOMBER was run over imagery pixels corresponding to water areas with bottom depths lower than 10 m as derived from the bathymetric IIM chart. The model was parameterized with intrinsic

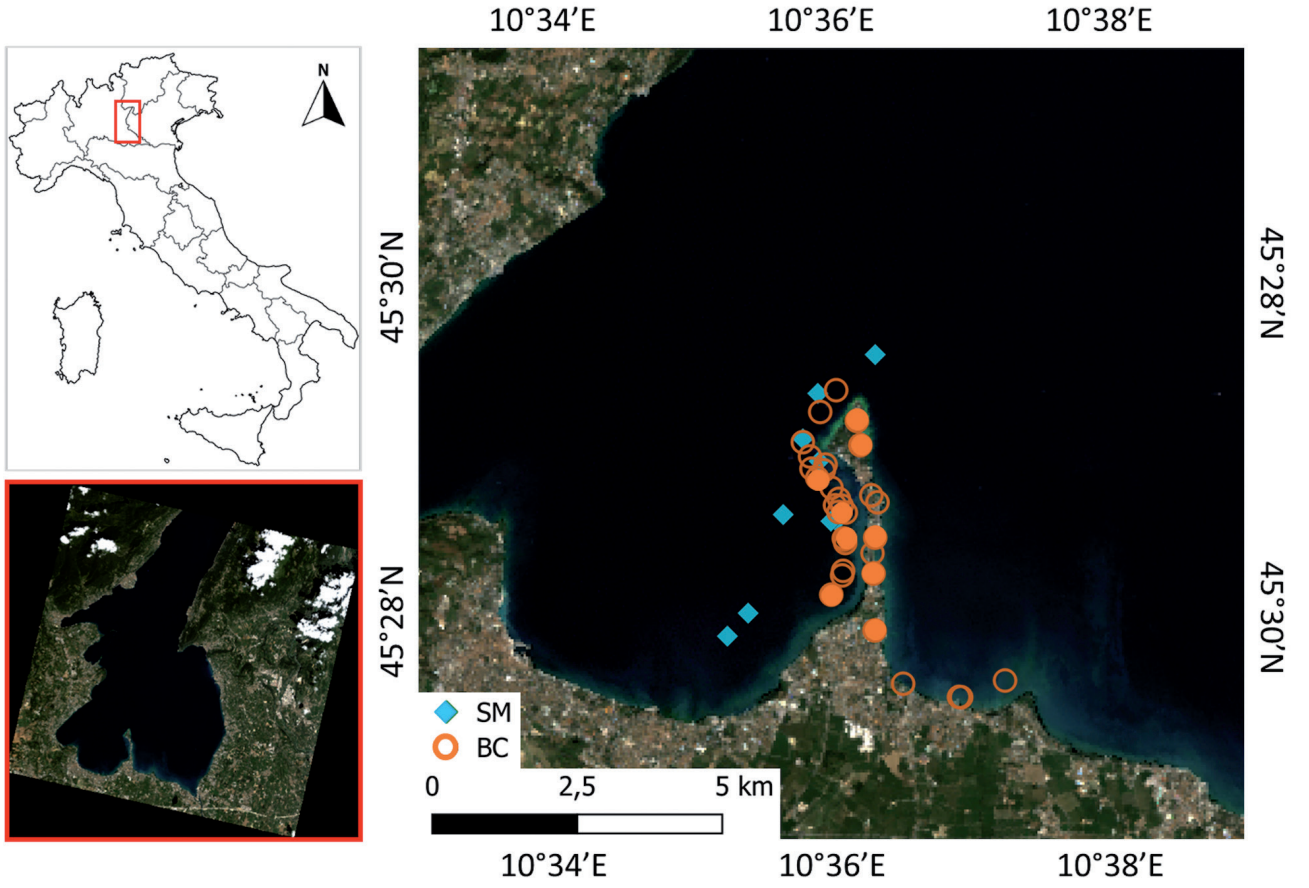


Fig. 1. On the left the location of Lake Garda at the top and the PRISMA true color image at the bottom, while on the right the data collected on 9th July 2024: in blue diamonds the spectral measurements (SM) and in orange circles the bottom classification data (BC). The filled orange circles identify stations where vegetation samples were collected.

OPEN ACCESS

optical properties specific for Lake Garda as in Ghirardi *et al*., (2022) apart for the reflectance of bottom types shown in Fig. 2. BOMBER was firstly run for bottom depth estimates and fc of two main components: sand and vegetation , as in Giardino *et al.* (2007) and in Ghirardi *et al.* (2019).. Subsequently, BOMBER was run separately for each of the two classes (sand and vegetation) to improve the level of detail in bottom classification where the first run was providing the predominant class of the substrate in terms of fc. Based on the results of this first run, pixels having a sand fc higher than 55% were labelled as mud, rock or *Dreissena bugensis* and *Dreissena polymorpha* (hereinafter referred to as *Dreissena* spp.). For pixels resulting with a vegetation fc >55% in the first run, a second run was performed to provide a more detailed classification of the colonized substrates of macrophytes as in Bresciani *et al.* (2012): dense (fc >70%), moderate (40% < fc <70%) and sparse macrophytes (fc <40%). The fc values obtained in the second run represent a new fc estimate and were therefore used independently from those obtained in the first run. Pixels for which neither sand nor vegetation was predominant in the first run were classified as 'mixed pixels'. The final map that BOMBER produced from the PRISMA pansh Rrs product consists of 7 bottom classes and depth.

Data validation and statistics

For the radiometric analysis, the PRISMA pansh Rrs were extracted from a 5x5 pixels window centred on each station. The mean value within this window was computed to reduce the noise (Zibordi *et al*., 2009; Concha *et al*., 2021). For each *in situ* station, multiple spectral signatures were acquired using WISP-3 and WISP-Orca within a ±1 h temporal window from the PRISMA overpass. These measurements were then averaged for each station and used as reference data for the validation of the PRISMA pansh image, acquired at 10:20 UTC.

Three descriptive statistics to assess the consistency between PRISMA and *in situ* radiometry were calculated as follows:

- Root-mean-square error (RMSE), a measure of the differences between values predicted by a model, or an estimator and the values observed:

$$RMSE\ (sr^{-1}) = \sqrt{\frac{\Sigma(x_i - y_i)^2}{n}} \quad \text{(Eq. 1)}$$

- Spectral angle (SA), a measure for directly comparing image spectra (PRISMA) to a known spectra (*in situ* data), and determine how similar the spectra shape are, computed in the range 0-180°:

$$SA\ (°) = \cos^{-1} \frac{\Sigma_{i=1}^{n} y_i x_i}{\sqrt{\Sigma_{i=1}^{n} y_i^2} \sqrt{\Sigma_{i=1}^{n} x_i^2}} \quad \text{(Eq. 2)}$$

- Median symmetric accuracy (*MdSA*), a robust method for estimating the spread of a multiplicative linear model using the log accuracy ratio; it can be interpreted as a percentage error, but it does not penalize overprediction and underprediction differently. It is often used instead of the common R^2 in ocean color studies where sample availability is often a limit (Pellegrino *et al*., 2023). It is defined as (Morley *et al*., 2018):

$$MdSA\ (\%) = 100 * (10^{M|log_{10}\left(\frac{y_i}{x_i}\right)|} - 1) \quad \text{(Eq. 3)}$$

The following statistics were used to validate the bathymetric maps, in addition to the RMSE (m^{-1}) mentioned above:

- Pearson's correlation coefficient (r), the correlation coefficient that measures linear correlation between two sets of data:

$$r\ (-) = \frac{cov(x_i, y_i)}{\sigma_{x_i} \sigma_{y_i}} \quad \text{(Eq. 4)}$$

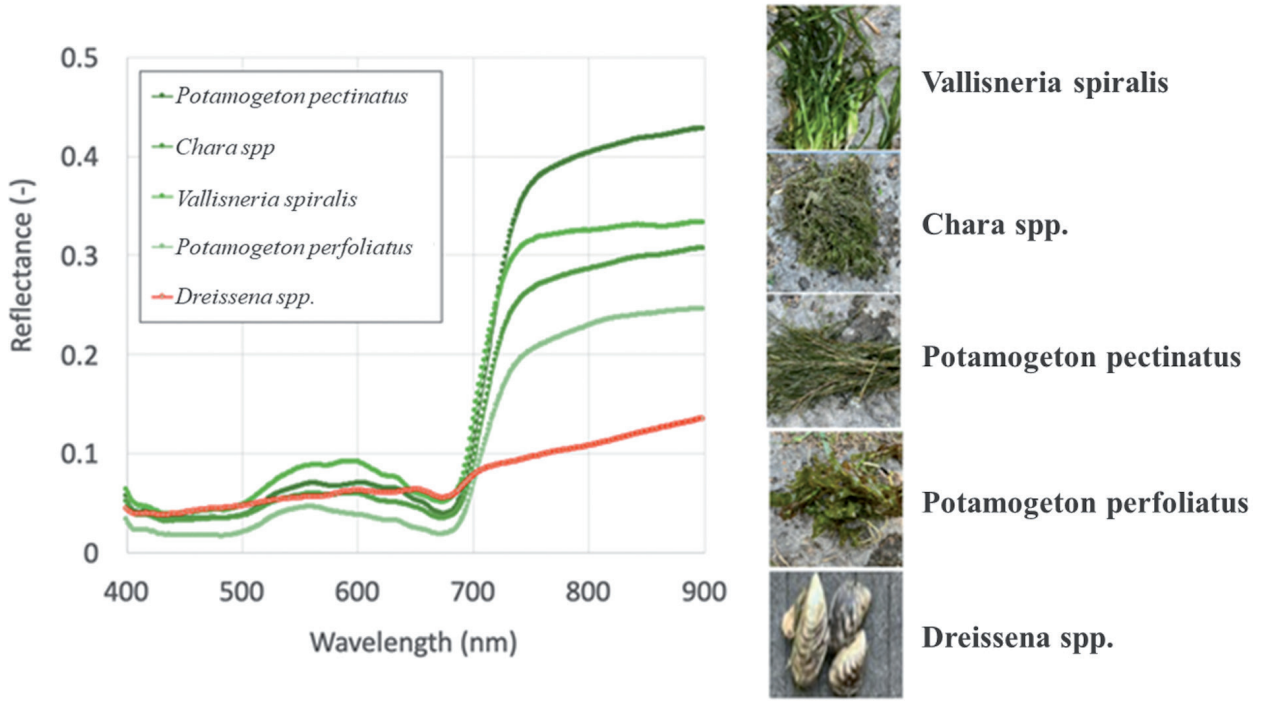


Fig. 2. Spectral reflectance of the main species colonizing Lake Garda substrates collected on 9th July 2024 in the 9 of the 32 stations defined in Fig. 1.

- Bias, a measure of the average tendency of the simulated values to be larger or smaller than their observed ones:

$$Bias\ (\%) = \frac{(x_i - y_i)}{x_i} * 100 \quad \text{(Eq. 5)}$$

- Mean Absolute Error, a measure of errors between paired observations expressing the same phenomenon:

$$MAE\ (m^{-1}) = \frac{\sum_{i=1}^{n} |y_i - x_i|}{n} \quad \text{(Eq. 6)}$$

Where: x_i are the measures from satellite sensor; y_i are the *in situ* measurements; $\bar{x}$ and $\bar{y}$ are the average values of the observations of x and y; n is the sample size; M is the median function; cov is the covariance.

For the validation of the bottom classification map, *in situ* observations of the substrate type at each sampling location were used as reference data. In total, 44 reference points were collected. Each *in situ* point was spatially matched to the corresponding pixel in the classification map (pixel-to-point comparison), and the assigned class was compared with the observed substrate type. Classification accuracy was assessed using the Overall Accuracy (OA), which measures the percentage of samples that are correctly classified (Ghirardi *et al*., 2019).

Pixel aggregation

Spatial pixel aggregation was performed to simulate the effect of progressively coarser spatial resolutions on the classification of benthic substrate classes and depth. Starting from the 5 m resolution classification map, generated by BOMBER from the PRISMA pansh product, two aggregated maps were generated at 10 m and 30 m spatial resolution as representative of pixel sizes typical of medium-resolution satellite sensors. The aggregation procedure used the "majority resampling" algorithm, whereby each output pixel at coarser spatial resolution was assigned to the modal class value (i.e., the most frequently occurring class) among all finer-resolution pixels within the corresponding aggregation block (Woodcock *et al*., 1988; Han *et al*., 2010). This approach represents one of the standard resampling technique for thematic raster data, as interpolation methods based on arithmetic averaging, such as bilinear or cubic resampling, are not suitable for discrete class labels (GDAL/OGR - https://www.osgeo.org/projects/gdal/; He *et al*., 2025). Furthermore, a dedicated mixed-pixel detection procedure was implemented to identify pixels located at the boundaries between distinct thematic groups, specifically between sand classes (rock, mud, and *Dreissena* spp.) and vegetation classes (dense, moderate, and sparse). Each aggregated pixel whose corresponding source block contained classes from both groups was labelled as "mixed pixels". This approach enables the mapping of mixed pixels as a function of spatial resolution, providing a direct assessment of how bigger pixel sizes progressively soften the boundaries between sand and vegetation, reducing the ability to discriminate individual benthic classes (Narayanan *et al*., 2002; Saura, 2004; Wang *et al*., 2020).

RESULTS AND DISCUSSION

Radiometry evaluation

As mentioned above, after assessing the quality of the pansharpening process, the quality controlled pansharpened PRISMA product with a 5 m pixel size, shown in Fig. S1, was evaluated radiometrically. The comparison between spectral signatures derived from the PRISMA pansh data and those collected *in situ* for optically shallow waters reveals an overall good agreement across the full spectrum. The mean spectral signatures show higher reflectance in the green region (around 550 nm), typical of turbid waters (Fabbretto *et al*., 2024), and greater discrepancies with *in situ* data in the blue region, as often happens with PRISMA data (Braga *et al*., 2022; Pellegrino *et al*., 2023). The agreement is also evident in the descriptive metrics: SA=11.2°, RMSE=0.0024 sr^{-1}, and MdSA=25%. Fig. 3 shows

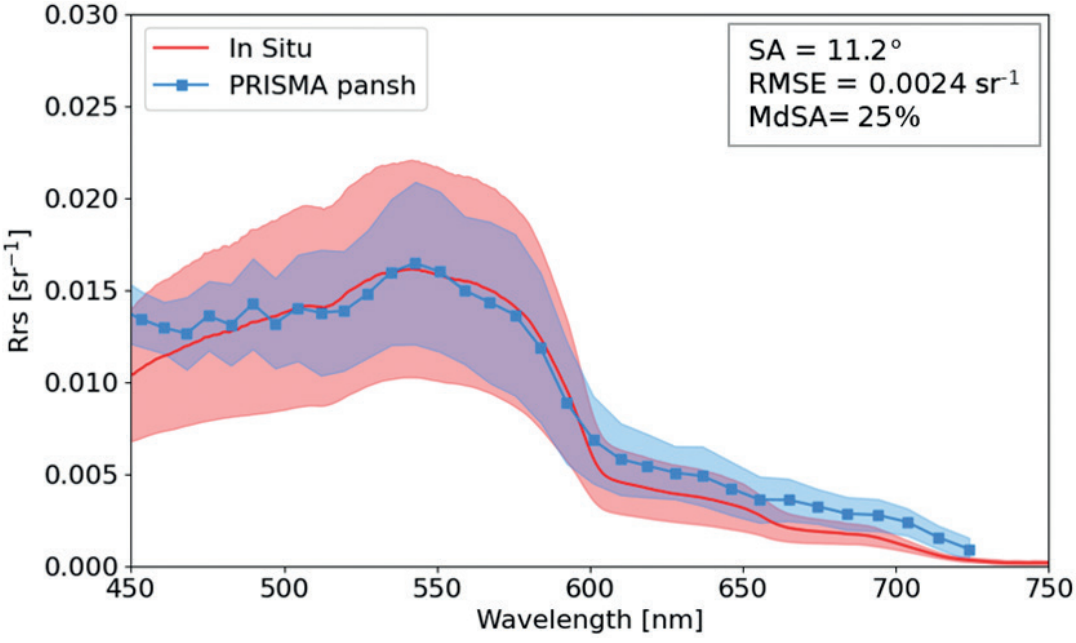


Fig. 3. Mean and standard deviation of spectral signatures retrieved on Lake Garda in optically shallow waters by PRISMA pansh product acquired on 9th July 2024 (blue line) and *in situ* instruments (red line).

OPEN ACCESS

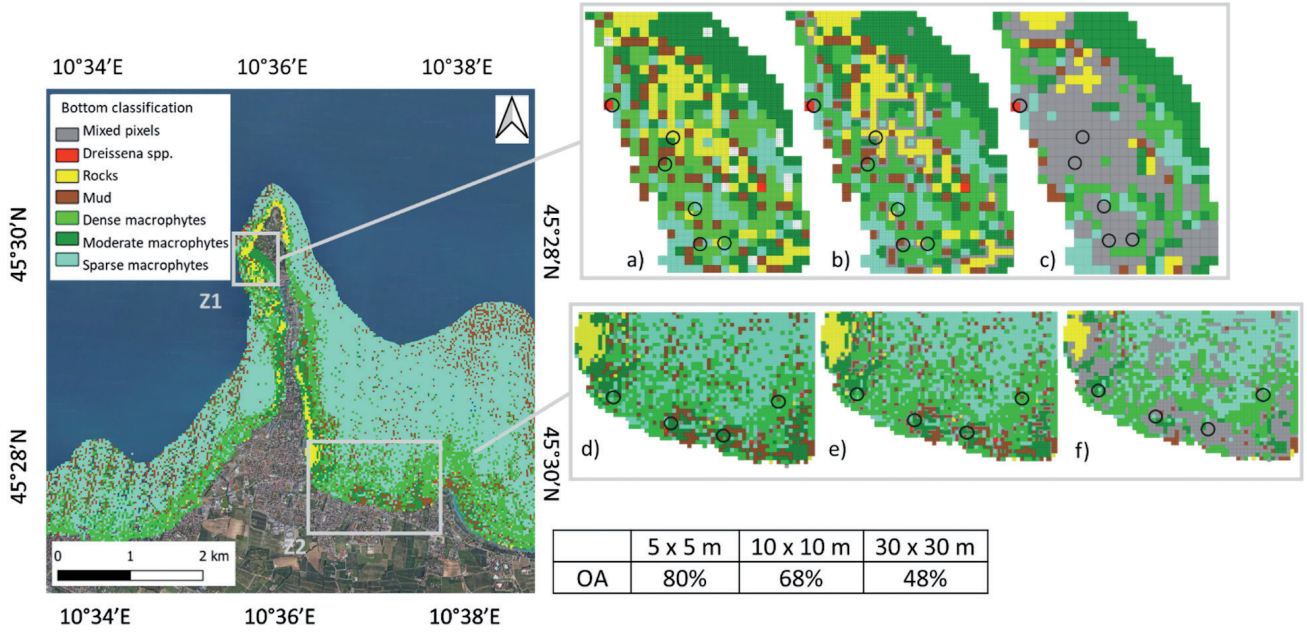
the mean of spectral signatures acquired at several stations across the study area, together with their standard deviation.

Bottom classification and bathymetric maps

The thematic map of the seven bottom type classes is shown in Fig. 4; the mapping is covering approximately 57 km², surrounding the Sirmione Peninsula, from the coastal line up to the 10 m isobath from the IIM chart. To assess how spatial resolution affects the generation of thematic maps, the additional products created by aggregating PRISMA pansh at 5 m to 10 and 30 m pixel sizes are also shown. Results are presented for two representative areas: Zone 1 (Z1) and Zone (Z2), that are located northwest and southeast of the Sirmione Peninsula, respectively. These zones were selected to highlight how pixel size influences the ability to discriminate among different bottom compositions. As resolution decreases from 5 m to 30 m, a clear loss of detail becomes evident. The proportion of mixed pixels increases substantially, especially in areas where multiple substrate types occur in close proximity (i.e., in Z1 from 3.5% in 5 x 5 m to 52% in 30 x 30 m). This effect is typical of optically shallow environments, where fine-scale heterogeneity, such as transitions between sand and macrophytes, can only be effectively captured at higher spatial resolutions. Coarser pixels tend to blend these features, reducing classification accuracy and potentially hiding ecologically relevant patterns. This phenomenon is even more evident in Z1, that is very heterogeneous due to the boat transit in the area, which limits the growth and colonization of macrophytes (Ghirardi *et al*., 2019). Additionally, in Fig. 4 (Z2), it is possible to observe how the *Dreissena* spp. class disappear at lower spatial resolution. Another example is the mud sample in Z1 (bottom left black circle), that is detected at 5 m and 10 m spatial resolution, but that gets lost at 30 m spatial resolution.

In Fig. 4, the OA for the area surrounding the Sirmione Peninsula is reported at 5 m, 10 m, and 30 m spatial resolutions. As spatial resolution decreases, OA also decreases: 80% at 5 m, 68% at 10 m, and 48% at 30 m. The confusion matrices for each product are presented in Fig. S2, Fig. S3 and Fig. S4, respectively. The results show, for example, that although only two *Dreissena* spp. samples are present, both are correctly identified at 5x5 m and at 10x10 m spatial resolutions, while one of the two samples is misclassified at 30x30 m. On the other hand, vegetation targets seem more difficult to distinguish among the three subclasses: dense, moderate and sparse. This may be due to subtle differences in their spectral signatures that are difficult to distinguish, as well as the presence of small patches where multiple species occur.

Fig. 5 shows the bottom depth retrieved from BOMBER together with the corresponding IIM isobaths chart, allowing for a visual comparison between the PRISMA-derived depths and the lakebed morphology from the high-resolution IIM field survey. A deeper channel, as already derived from airborne data at 5 m spatial resolution (Giardino *et al*., 2007a), is visible in the northwest portion near the coast (Z1), which allows ferries to reach the pier. Fig. 6 presents the validation results for datasets at 5 m, 10 m, and 30 m spatial resolution. The validation was conducted with respect to the IIM data (blue box, top left), the *in situ* bottom depths (orange box, below), and the combined dataset (black box, bottom right). As spatial resolution decreases, the accuracy of the depth retrieval also diminish, from r=0.82 to r=0.75, considering the two datasets combined. This reduction is primarily due to the coarser pixel size, which increases spectral mixing within each pixel. In addition, the agreement between bottom depth derived from BOMBER and *in situ* measurements collected during the field campaign appears to be higher than that obtained using IIM data (e.g., r=0.87 *vs* r=0.81 for the 5 m image, and r=0.75 *vs* r=0.74 for the 30 m image). This difference is likely related to the acquisition method: IIM surveys are conducted using an echo sounder (Zanone *et al*., 2021), which, although highly accurate, has limita-



	5 x 5 m	10 x 10 m	30 x 30 m
OA	80%	68%	48%

Fig. 4. Bottom type classification up to 10 m depth. On the upper right the Z1, on the bottom right the Z2. Data at 5 m spatial resolution (a,d), at 10 m (b,e), and at 30 m (c,f). Black circles identify the sampling points (bottom classification stations shown in Fig. 1).

tions in very shallow waters (approximately <2-5 m) due to vessel constraints. In fact, it can be seen that at the 5 m depth (Fig. 6a), the statistical differences between the two validations are much greater than those at 30 m (Fig. 6c).

Fig. 7 illustrates the distribution of the benthic classes along depth across the entire study area. The analysis was performed by associating each pixel of the 5 m resolution benthic classification with the corresponding bathymetric value; therefore, the distributions shown are based on the full classified area. The Kernel Density Estimation (KDE) was calculated separately for each benthic class using bathymetric values below the 90th percentile of each class distribution, to minimize the influence of outliers, i.e., anomalous values compared to neighboring pixels, often caused by mixed pixels or specular reflection. Dense, moderate, and sparse

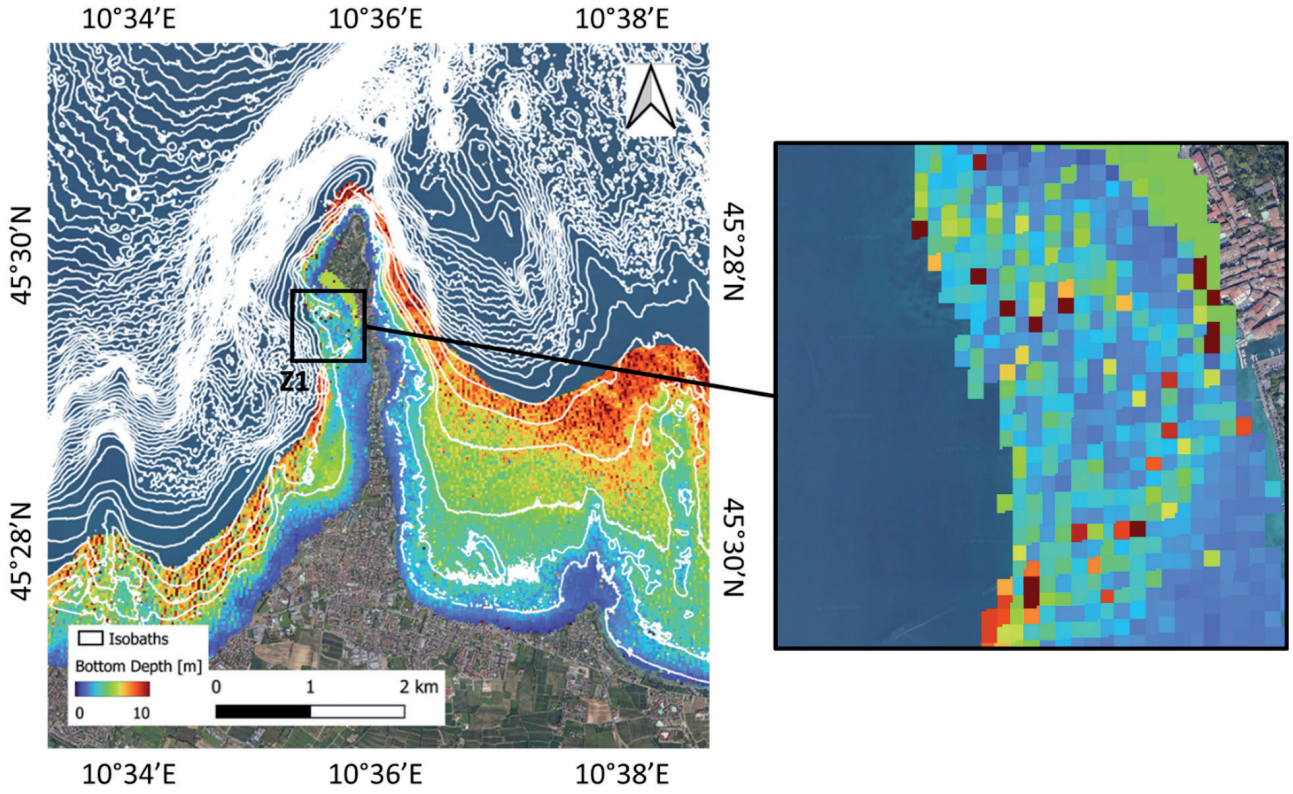


Fig. 5. Bottom depth map expressed in meters (zoom on the right) for the shallow waters around Sirmione Peninsula. In white the Isobaths defined by the IIM data.

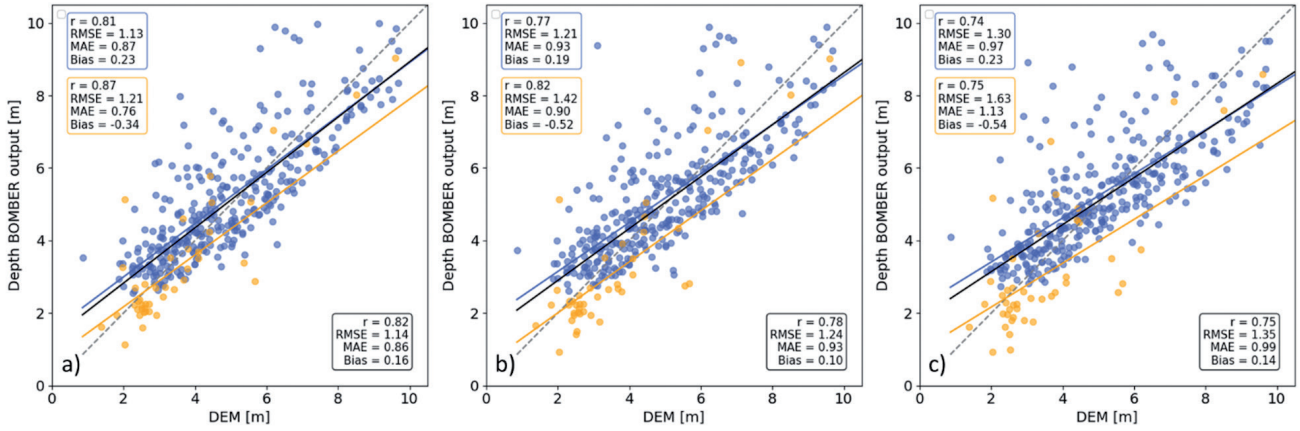


Fig. 6. Bottom depth validation for 5 m (a), 10 m (b) and 30 m (c), with validation statistics: r (-), RMSE (m^{-1}), MAE (m^{-1}), Bias (%).

OPEN ACCESS

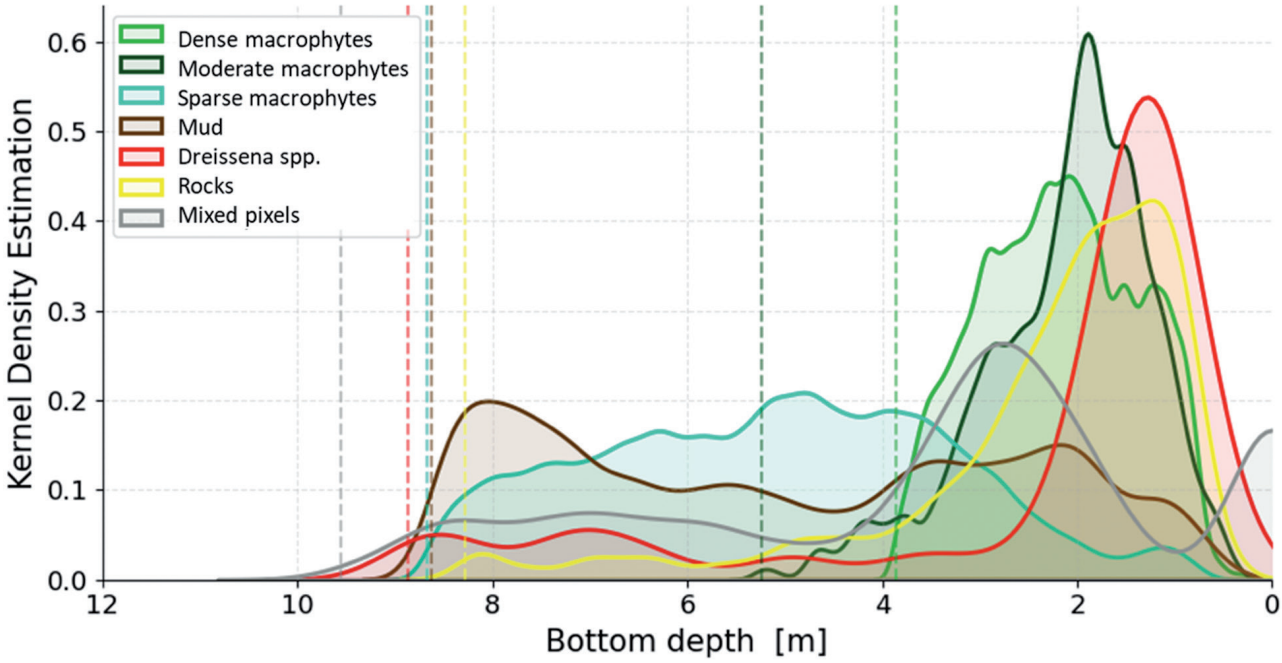


Fig. 7. Kernel Density Estimation chart for each benthic class, respect to bottom depth.

macrophytes are predominantly associated with shallow depths, with moderate macrophytes peaking at the very surface (1.5 m), dense macrophytes occurring slightly deeper (2 m), and sparse macrophytes spanning a broader range due to their greater tolerance to reduced light. Light is in fact one of the main drivers controlling the maximum depth at which macrophytes exist in aquatic ecosystems; in addition, its availability is directly affected by water colour, suspended matter, and the exponential attenuation of irradiance with depth (Liu *et al*., 2016). In contrast, mud becomes increasingly common with depth (8 m), reflecting sediment accumulation in low-energy environments (Potter *et al*., 2005), while *Dreissena* spp. is present at intermediate to deeper depths, consistent with its ability to colonize stable substrates under low-light conditions (Grutters *et al*., 2012), with peaks at 1 m depth. Rocky substrates show a more irregular pattern linked to lakebed morphology, and mixed pixels represent transitional or heterogeneous areas (Yu *et al*., 2018).

CONCLUSIONS

High spatial resolution data offer critical advantages for the detailed mapping of aquatic environments. They also enable the observation of heterogeneous targets, when combined with high spectral resolution, like has been achieved by airborne imaging spectrometry for decades. In this study, a shallow water ecosystem in a lake with clear water was characterized using PRISMA pansh products, which allowed the classification of substrate properties in terms of substrate types, cover and vegetation density, as well as bottom depth. This fine-scale, spatially distributed information can complement conventional water sampling, to enlarge the spatial coverage and hence support the reporting on the ecological status of the aquatic ecosystems; in particular, EC 2000/60 of the Water Framework Directive (WFD) requires the monitoring of the abundance and composition of macrophytes (Bolpagni *et al*., 2017).

A pixel-based aggregation procedure over the high-resolution PRISMA-derived shallow water products allowed to assess the increasing of errors moving from 5 m to 30 m spatial resolution. The study enabled high fidelity mapping from fused HYC and PAN PRISMA images. Further study is required to address the common requirements of fine-scale mapping in heterogeneous and optically complex targets. To the aim, the need of fusing HYC and PAN may benefit from other procedures able to ingest not only L2D products, but also BOA reflectance obtained with other atmospheric correction models. As PRISMA is the only satellite sensor so far simultaneously acquiring HYC and PAN data at GSD of 30 m and 5 m respectively, the opportunities of improving the processing methods and of enabling application remains somehow limited in terms of both temporal and geographic coverage. Yet, like other precursors, the PRISMA mission offers opportunities to develop studies supporting novel satellite missions for observing aquatic ecosystems and to develop applications requiring high spectral and spatial resolution, such as quantifying material exchanges across land-water boundary ecosystems and assessing shifts in species distribution (Chami *et al*., 2025).

REFERENCES

Aiazzi B, Alparone L, Baronti S, Garzelli A, Selva M, 2013. Pansharpening of hyperspectral images: a critical analysis of requirements and assessment on simulated PRISMA. Proc. SPIE 8892, Image and Signal Processing for Remote Sensing XIX, 889203.

Alparone L, Aiazzi B, Baronti S, Garzelli A, 2015. Remote sensing image fusion. CRC Press, Boca Raton: 324 pp.

Asplund TR, Cook CM, 1997. Effects of motor boats on submerged aquatic macrophytes. Lake Reserv Manag 13:1-12.

Badiani B, Barontini S, Bettoni B, Bonati S, Peli M, Pietta A, et al., 2017. Lake Garda lemon houses (Italy): Opportunities of a sensitive, marginal area in urban planning. Change Adapt Socio-Ecol Syst 3:111-118.

Bandara WGC, Valanarasu JMJ, Patel VM, 2021. Hyperspectral pansharpening based on improved deep image prior and residual reconstruction. IEEE Trans Geosci Remote Sens 60:5520816.

Begliomini FN, Barbosa CCF, Martins VS, Novo EMLM, Paulino RS, Maciel DA, et al., 2023. Machine learning for cyanobacteria mapping on tropical urban reservoirs using PRISMA hyperspectral data. ISPRS J Photogramm Remote Sens 204: 378-396.

Bell TW, Cavanaugh KC, Saccomanno VR, Cavanaugh KC, Houskeeper HF, Eddy N, et al., 2023. Kelpwatch: A new visualization and analysis tool to explore kelp canopy dynamics reveals variable response to and recovery from marine heatwaves. PLoS One 18:e0271477.

Belluco E, Camuffo M, Ferrari S, Modenese L, Silvestri S, Marani A, et al., 2006. Mapping salt-marsh vegetation by multispectral and hyperspectral remote sensing. Remote Sens Environ 105: 54-67.

Bertrin V, Boutry S, Alard D, Haury J, Jan G, Moreira S, et al., 2018. Prediction of macrophyte distribution: The role of natural versus anthropogenic physical disturbances. Appl Veg Sci 21:395-410.

Bolpagni R, Azzella MM, Agostinelli C, Beghi A, Bettoni E, Brusa G, et al., 2017. Integrating the Water Framework Directive into the Habitats Directive: analysis of distribution patterns of lacustrine EU habitats in lakes of Lombardy (northern Italy). J Limnol 76:1627.

Bolpagni R, Bettoni E, Bonomi F, Bresciani M, Caraffini K, Costaraoss S, et al., 2013. Charophytes of the lake Garda (Northern Italy): a preliminary assessment of diversity and distribution. J Limnol 72:e31.

Braga F, Fabbretto A, Vanhellemont Q, Bresciani M, Giardino C, Scarpa GM, et al., 2022. Assessment of PRISMA water reflectance using autonomous hyperspectral radiometry. ISPRS J Photogramm Remote Sens 192:99-114.

Braga F, Giardino C, Bassani C, Matta E, Candiani G, Strömbeck N, et al., 2013. Assessing water quality in the northern Adriatic Sea from HICO™ data. Remote Sens Lett 4:1028-1037.

Bresciani M, Bolpagni R, Braga F, Oggioni A, Giardino C, 2012. Retrospective assessment of macrophytic communities in southern Lake Garda (Italy) from in situ and MIVIS (Multispectral Infrared and Visible Imaging Spectrometer) data. J Limnol 71:e19.

Bresciani M, Sotgia C, Fila GL, Musanti M, Bolpagni R, 2011. Assessing common reed bed health and management strategies in Lake Garda (Italy) by means of Leaf Area Index measurements. Ital J Remote Sens 43:75-86.

Chami M, Bracher A, Briottet X, Costa M, Damm-Reiser A, Dekker A, et al., 2025. GALENE: A proposed future satellite mission dedicated to the observation of coastal and inland aquatic ecosystems, including the monitoring of water quality and the detection of marine plastics. Proc. One Ocean Science Congress; abstract OOS2025-262.

Ciotola M, Vitale S, Mazza A, Poggi G, Scarpa G, 2022. Pansharpening by convolutional neural networks in the full resolution framework. IEEE Trans Geosci Remote Sens 60:1-17.

Ciutti F, Beltrami ME, Confortini I, Cianfanelli S, Cappelletti C, 2011. Non-indigenous invertebrates, fish and macrophytes in Lake Garda (Italy). J Limnol 70:315.

Cogliati S, Sarti F, Chiarantini L, Cosi M, Lorusso R, Lopinto E, et al., 2021. The PRISMA imaging spectroscopy mission: overview and first performance analysis. Remote Sens Environ 262:112499.

Concha JA, Bracaglia M, Brando VE, 2021. Assessing the influence of different validation protocols on Ocean Colour match-up analyses. Remote Sens Environ 259:112415.

Corbari L, Capodici F, Ciraolo G, Topouzelis K, 2023. Marine plastic detection using PRISMA hyperspectral satellite imagery in a controlled environment. Int J Remote Sens 44:6845-6859.

Fabbretto A, Bresciani M, Pellegrino A, Alikas K, Pinardi M, Mangano S, et al., 2024. Tracking water quality and macrophyte changes in Lake Trasimeno (Italy) from spaceborne hyperspectral imagery. Remote Sens 16:1704.

Gasith A, Hoyer MV, 1998. Structuring role of macrophytes in lakes: changing influence along lake size and depth gradients. pp. 381-392.

Ghirardi N, Bolpagni R, Bresciani M, Valerio G, Pilotti M, Giardino C, 2019. Spatiotemporal dynamics of submerged aquatic vegetation in a deep lake from Sentinel-2 data. Water 11:563.

Ghirardi N, Bresciani M, Free G, Pinardi M, Bolpagni R, Giardino C, 2022. Evaluation of macrophyte community dynamics (2015–2020) in southern Lake Garda (Italy) from Sentinel-2 data. Appl Sci 12:2693.

Giardino C, Bartoli M, Candiani G, Pellegrini L, 2007a. Recent changes in macrophyte colonisation patterns: an imaging spectrometry-based evaluation of southern Lake Garda (northern Italy). J Appl Remote Sens.

Giardino C, Brando VE, Dekker AG, Strömbeck N, Candiani G, 2007b. Assessment of water quality in Lake Garda (Italy) using Hyperion. Remote Sens Environ 109:183-195. https://doi.org/10.1016/j.rse.2006.12.017.

Giardino C, Bresciani M, Cazzaniga I, Schenk K, Rieger P, Braga F, et al., 2014. Evaluation of multi-resolution satellite sensors for assessing water quality and bottom depth of Lake Garda. Sensors 14:24116-24131.

Giardino C, Candiani G, Bresciani M, Lee Z, Gagliano S, Pepe M, 2012. BOMBER: A tool for estimating water quality and bottom properties from remote sensing images. Comput Geosci 45:313-318.

Giardino C, Pahlevan N, Fabbretto A, Panizza L, Pellegrino A, Vandermeulen R, et al., 2025. ACIX-III Aqua: evaluation of atmospheric correction for hyperspectral PRISMA imagery over inland and coastal waters. Int J Remote Sens:1-25.

Goffi G, Osti L, Nava CR, Maurer O, Pencarelli T, 2021. Is preservation the key to quality and tourists' satisfaction? Evidence from Lake Garda. Tour Recreat Res 46:434-440.

Grutters BMC, Verhofstad MJJM, van der Velde G, Rajagopal S, Leuven RSEW, 2012. A comparative study of byssogenesis on zebra and quagga mussels: the effects of water temperature, salinity and light–dark cycle. Biofouling 28:121-129.

Han P, Li Z, Gong J, 2010. Effects of aggregation methods on image classification. In: Geospatial technology for Earth observation, p. 271-288. In: Li D, Shan J, Gong J (eds.), Geospatial Technology for Earth Observation. Springer.

He L, Zhu J, Li J, Meng D, Chanussot J, Plaza A, 2020. Spectral-fidelity convolutional neural networks for hyperspectral pansharpening. IEEE J Sel Top Appl Earth Obs Remote Sens 13:5898-5914.

He L, Zhu J, Li J, Plaza A, Chanussot J, Li B, 2019. HyperPNN: Hyperspectral pansharpening via spectrally predictive convolutional neural networks. IEEE J Sel Top Appl Earth Obs Remote Sens 12:3092-3100.

OPEN ACCESS

Hestir EL, Khanna S, Andrew ME, Santos MJ, Viers JH, Greenberg JA, et al., 2008. Identification of invasive vegetation using hyperspectral remote sensing in the California Delta ecosystem. Remote Sens Environ 112:4034-4047.

He X, Zhou C, Gao M, Sun S, Lyu C, Han X, 2025. A method for preserving three spatial features in the upscaling of categorical raster data. Comput Geosci 201:105933.

Hinegk L, Adami L, Piccolroaz S, Amadori M, Moretti M, Tubino M, et al., 2023. Multidecadal analysis of Lake Garda water balance. J Limnol 82:2144.

Hinegk L, Adami L, Zolezzi G, Tubino M, 2022. Implications of water resources management on the long-term regime of Lake Garda (Italy). J Environ Manage 301:113893.

Hommersom A, Kratzer S, Laanen M, Ansko I, Ligi M, Bresciani M, et al., 2012. Intercomparison in the field between the new WISP-3 and other radiometers (TriOS Ramses, ASD FieldSpec, and TACCS). J Appl Remote Sens 6:063615.

Kapakasa F, Adetunji A, Chisenga C, 2024. An integrated analysis of aeromagnetic and PRISMA hyperspectral imagery data for potential gold mineralization exploration in Mwanza, Malawi. Arab J Geosci 17:241.

Lee Z, Carder KL, Mobley CD, Steward RG, Patch JS, 1999. Hyperspectral remote sensing for shallow waters: 2. Deriving bottom depths and water properties by optimization. Appl Opt 38:3831.

Lesiv MS, Polishchuk AI, Antonyak HL, 2020. Aquatic macrophytes: ecological features and functions. Stud Biol 14:79-94.

Liu X, Zhang Y, Shi K, Lin J, Zhou Y, Qin B, 2016. Determining critical light and hydrologic conditions for macrophyte presence in a large shallow lake: The ratio of euphotic depth to water depth. Ecol Indic 71:317-326.

Loizzo R, Guarini R, Longo F, Scopa T, Formaro R, Facchinetti C, et al., 2018. PRISMA: The Italian hyperspectral mission. Proc. IEEE Int. Geoscience and Remote Sensing Symp., Valencia; pp. 175-178.

Loncan L, de Almeida LB, Bioucas-Dias JM, Briottet X, Chanussot J, Dobigeon N, et al., 2015. Hyperspectral pansharpening: A review. IEEE Geosci Remote Sens Mag 3:27-46.

Masi G, Cozzolino D, Verdoliva L, Scarpa G, 2016. Pansharpening by convolutional neural networks. Remote Sens 8:594.

Meerhoff M, de los Ángeles González-Sagrario M, 2021. Habitat complexity in shallow lakes and ponds: importance, threats, and potential for restoration. Hydrobiologia 849:3737-3760.

Morley SK, Brito TV, Welling DT, 2018. Measures of model performance based on the log accuracy ratio. Space Weather 16:69-88.

Mueller JL, Austin RW, Fargion GS, McClain CR, 2000. Ocean optics protocols for satellite ocean color sensor validation. National Aeronautics and Space Administration, Goddard Space Flight Center, Greenbelt.

Musto R, Tricomi A, Bruno R, Pasquali G, 2023. Advancing PRISMA pansharpening: A deep learning approach with synthetic data pretraining and transfer learning. Proc.13th Workshop on Hyperspectral Imaging and Signal Processing: Evolution in Remote Sensing (WHISPERS); pp. 1-7.

Musto R, Tricomi A, Bruno R, Pasquali G, 2024. Convolutional attention module for PRISMA pansharpening in the guided full resolution framework. Proc. IEEE Int. Geoscience and Remote Sensing Symp., Athens; pp. 1222-1225.

Narayanan RM, Desetty MK, Reichenbach SE, 2002. Effect of spatial resolution on information content characterization in remote sensing imagery based on classification accuracy. Int J Remote Sens 23:537-553.

Olmanson LG, Brezonik PL, Bauer ME, 2015. Remote sensing for regional lake water quality assessment: capabilities and limitations of current and upcoming satellite systems, pp. 111-140. In: Younos T, Parece T (eds.), Advances in Watershed Science and Assessment. Springer.

O'Shea RE, Pahlevan N, Smith B, Bresciani M, Egerton T, Giardino C, et al., 2021. Advancing cyanobacteria biomass estimation from hyperspectral observations: Demonstrations with HICO and PRISMA imagery. Remote Sens Environ 266:112693.

Park J, Lee H, Asselman J, Janssen C, Depuydt S, De Saeger J, et al., 2024. Harnessing the power of tidal flat diatoms to combat climate change. Crit Rev Environ Sci Technol 54:1395-1416.

Pellegrino A, Fabbretto A, Bresciani M, de Lima TMA, Braga F, Pahlevan N, et al., 2023. Assessing the accuracy of PRISMA standard reflectance products in globally distributed aquatic sites. Remote Sens 15:2163.

Potter PE, Maynard JB, Depetris PJ, 2005. Mud and mudstones: Introduction and overview. Springer, Berlin.

Rubio R, Paná S, Nemiña F, Fabbretto A, Ferral A, Bresciani M, et al., 2025. Assessing the potentiality of UFSAT-1 in TOA radiance and BOA reflectance for inland waters. Proc. Latin American GRSS & ISPRS Remote Sensing Conf., Foz do Iguaçu; pp. 1-7.

Ruddick KG, Bialek A, Brando VE, De Vis P, Dogliotti AI, Doxaran D, et al., 2024a. HYPERNETS: a network of automated hyperspectral radiometers to validate water and land surface reflectance (380–1680 nm) from all satellite missions. Front Remote Sens 5:1372085.

Ruddick KG, Brando VE, Corizzi A, Dogliotti AI, Doxaran D, Goyens C, et al., 2024b. WATERHYPERNET: a prototype network of automated in situ measurements of hyperspectral water reflectance for satellite validation and water quality monitoring. Front Remote Sens 5: 1347520.

Sagerman J, Hansen JP, Wikström SA, 2020. Effects of boat traffic and mooring infrastructure on aquatic vegetation: A systematic review and meta-analysis. Ambio 49:517-530.

Salmaso N, Boscaini A, Capelli C, Cerasino L, 2018. Ongoing ecological shifts in a large lake are driven by climate change and eutrophication: evidences from a three-decade study in Lake Garda. Hydrobiologia 824:177-195.

Salmaso N, Mosello R, 2010. Limnological research in the deep southern subalpine lakes: synthesis, directions and perspectives. Adv Oceanogr Limnol 1:29-66.

Salmaso N, Padisák J, 2007. Morpho-functional groups and phytoplankton development in two deep lakes (Lake Garda, Italy and Lake Stechlin, Germany). Hydrobiologia 578:97-112.

Saura S, 2004. Effects of remote sensor spatial resolution and data aggregation on selected fragmentation indices. Landsc Ecol 19:197-209.

Schoelynck J, Creëlle S, Buis K, De Mulder T, Emsens WJ, Hein T, et al., 2018. What is a macrophyte patch? Patch identification in aquatic ecosystems and guidelines for consistent delineation. Ecohydrol Hydrobiol 18:1-9.

Schütt EM, Uhl F, Schubert PR, Reusch TBH, Oppelt N, 2025. Mapping subtidal seagrass in the turbid Baltic Sea: Rethinking satellite sensor selection using a sensor-agnostic pipeline. Sci Remote Sens 11:100243.

Taggio N, Aiello A, Ceriola G, Kremezi M, Kristollari V, Kolokoussis P, et al., 2022. A combination of machine learning algorithms for marine plastic litter detection exploiting hyperspectral PRISMA data. Remote Sens 14:3606.

Thomaz SM, 2023. Ecosystem services provided by freshwater macrophytes. Hydrobiologia 850:2757-2777.

Thomaz SM, Cardozo ALP, Quirino BA, Yofukuji KY, Aleixo MHF, Fugi R, 2025. A review of the ecological role of aquatic macrophytes on freshwater fish. Hydrobiologia 852:3257-3290.

Vabson V, Kuusk J, Ansko I, Vendt R, Alikas K, Ruddick K, et al., 2019. Laboratory intercomparison of radiometers used for satellite validation in the 400–900 nm range. Remote Sens 11:1101.

Villamagna AM, Murphy BR, 2010. Ecological and socio-economic impacts of invasive water hyacinth (*Eichhornia crassipes*): a review. Freshwater Biol 55:282-298.

Villa P, Laini A, Bresciani M, Bolpagni R, 2013. A remote sensing approach to monitor the conservation status of lacustrine *Phragmites australis* beds. Wetl Ecol Manag 21:399-416.

Vivone G, Alparone L, Chanussot J, Dalla Mura M, Garzelli A, Licciardi GA, et al., 2015. A critical comparison among pansharpening algorithms. IEEE Trans Geosci Remote Sens 53:2565-2586.

Vivone G, Garzelli A, Xu Y, Liao W, Chanussot J, 2023. Panchromatic and hyperspectral image fusion: Outcome of the 2022 WHISPERS Hyperspectral Pansharpening Challenge. IEEE J Sel Top Appl Earth Obs Remote Sens 16:166-179.

Wald L, Ranchin T, Mangolini M, 1997. Fusion of satellite images of different spatial resolutions: Assessing the quality of resulting images. Photogramm Eng Remote Sens 63:691-699.

Wang Q, Shi W, Atkinson PM, 2020. Information loss-guided multi-resolution image fusion. IEEE Trans Geosci Remote Sens 58: 45-57.

Woodcock CE, Strahler AH, Jupp DLB, 1988. The use of variograms in remote sensing: I. Scene models and simulated images. Remote Sens Environ 25:323-348.

Yang J, Fu X, Hu Y, Huang Y, Ding X, Paisley J, 2017. PanNet: A deep network architecture for pan-sharpening. Proc. IEEE Int. Conf. on Computer Vision (ICCV), Venice; pp. 1753-1761.

Yu W, Li J, Liu Q, Zeng Y, Zhao J, Xu B, et al., 2018. Global land cover heterogeneity characteristics at moderate resolution for mixed pixel modeling and inversion. Remote Sens 10:856.

Zanone E, Biscotti E, Monaca A, Pucci M, 2021. Inland water hydrographic survey for mapping and scientific research. ICA-Abs 3:325.

Zheng Y, Li J, Li Y, Guo J, Wu X, Chanussot J, 2020. Hyperspectral pansharpening using deep prior and dual attention residual network. IEEE Trans Geosci Remote Sens 58:8059-8076.

Ziaja M, Kowaleczko P, Tarasiewicz T, Kostrzewa D, Kawulok M, 2025. Hyperspectral pansharpening enhanced with multi-image super-resolution for PRISMA data. IEEE J Sel Top Appl Earth Obs Remote Sens 18:16562-16578.

Zibordi G, Berthon JF, Mélin F, D'Alimonte D, Kaitala S, 2009. Validation of satellite ocean color primary products at optically complex coastal sites: Northern Adriatic Sea, Northern Baltic Proper and Gulf of Finland. Remote Sens Environ 113:2574-2591.

Online supplementary material:

Fig. S1. PRISMA pansh product.

Fig. S2. Confusion matrix for the 5x5 m spatial resolution PRISMA pansh classificated product.

Fig. S3. Confusion matrix for the 10x10 m spatial resolution PRISMA pansh classificated product.

Fig. S4. Confusion matrix for the 30x30 m spatial resolution PRISMA pansh classificated product.

Received: 29 June 2026; Accepted: 18 October 2026.

Contributions: Lodovica Panizza, conceptualization, methodology, validation, formal analysis, investigation, data curation, writing - original draft preparation, writing - review & editing. Mariano Bresciani, conceptualization, methodology, validation, formal analysis, investigation, data curation, writing - original draft preparation, writing - review & editing, supervision. Alessia Tricomi, methodology, validation, data curation, writing - review & editing, supervision. Federica Braga, writing - review & editing. Andrea Pellegrino, data curation, writing - review & editing. Alice Fabbretto, writing - review & editing. Riccardo Musto, data curation, writing - review & editing. Cecilia Sciarretta, data curation, writing - review & editing. Claudia Giardino, conceptualization, methodology, validation, investigation, data curation, writing - original draft preparation, writing - review & editing, supervision. All authors have read and agreed to the published version of the manuscript.

Conflict of interest: the authors declare no competing interests, and all authors confirm accuracy.

Data Availability Statement: the datasets used and/or analysed during the current study are available from the corresponding author upon reasonable request. This excludes PRISMA products of the Italian Space Agency (ASI) that were delivered for this study under an ASI License to use.

Funding: part of this work was supported by ASI-CNR, n. 20195HH0 (Attività scientifica di CAL/VAL della missione PRISMA, PRISCAV); Space It Up project funded by the Italian Space Agency (ASI) and the Ministry of University and Research (MUR), under contract n. 2024-5-E.0 - CUP n. I53D24000060005 and ASI "PRISMA SCIENZA" (DC-UOT-2019-061) PANDA-WATER "PRISMA Products AND Applications for inland and coastal WATER" [Contract/Agreement n. 2022-15-U.0, CUP F73C22000790005].

Acknowledgments: the high-resolution bathymetry of Lake Garda was provided by the Hydrographic Institute of the Italian Navy (IIM) and realized within the project ACCURATE (https://asa.unicatt.it/asa-progetti-accurate) in collaboration with the Catholic University of Sacred Heart (UNICAT, Brescia). PRISMA data were used upon agreement of respective licenses to use. We are very grateful to S. Mangano and M. Musanti for the fieldwork activity. All fieldwork was made possible thanks to the CNR-IREA Eugenio Zilioli Experimental Station in Sirmione, which is part of the LTER network, and thanks to the collaboration with the Municipality of Sirmione. We would like to thank the two anonymous reviewers for their insightful comments that helped strengthening this manuscript.

Publisher's note: all claims expressed in this article are solely those of the authors and do not necessarily represent those of their affiliated organizations, or those of the publisher, the editors and the reviewers. Any product that may be evaluated in this article or claim that may be made by its manufacturer is not guaranteed or endorsed by the publisher.

This work is licensed under a Creative Commons Attribution-NonCommercial 4.0 International License (CC BY-NC 4.0).